www.czasopisma.pan.pl PAN POLSKA AKADEMIA NAUK www.journals.pan.pl

Arch. Min. Sci. **69** (2024), 2, 175-190

Electronic version (in color) of this paper is available: http://mining.archives.pl

DOI: https://doi.org/10.24425/ams.2024.150340

FAXIONG CAI[1], WEI SUN[1,2*], SHENGYOU ZHANG[1], AILUN ZHU[1], FANYU DING[1], PANKE ZHANG[1], YAO WEN[1], SHAOYONG WANG[3], YINGKUI XIAO[4]

STRENGTH AND CRACK PROPAGATION ANALYSIS OF LAYERED BACKFILL BASED ON ENERGY THEORY

The strength of backfill is greatly influenced by its inclination angle and interlayer concentration. In order to study the influence of inclination angle and interlayer mass concentration on the strength of backfill, a group of layered cemented backfill with cement-sand ratio of 1:4, interlayer mass concentration of 66%, 67% and 68% and inclination angles of 0°, 10°, 20° and 30° were prepared by using tailings as aggregate. The uniaxial compression test was carried out to analyse the effect of interlayer mass concentration and inclination angle on layered cemented backfill. The crack propagation and energy change law of the specimen during compression were analysed by J-integral and energy conservation law. The relationship between the crack initiation and propagation and strain energy of two representative three-layer backfill specimens was analysed by numerical modelling. The results show that the increase in the layer number and the inclination angle of the backfill can weaken the strength of the backfill. In a certain range of inclination angles, the weakening coefficient of the backfill caused by the inclination angle is very consistent with the cosine value of the corresponding angle. Due to the release of crack energy and the existence of interface J integral, the uniaxial compressive strength of different mass concentration backfill is different at various positions. When the displacement reaches a certain value, the crack and strain energy no longer increase.

Keywords: cemented tailings backfill; conservation of energy; J-integral; uniaxial compressive strength; contact angle

[1] KUNMING UNIVERSITY OF SCIENCE AND TECHNOLOGY, FACULTY OF LAND AND RESOURCES ENGINEERING KUNMING 650093, CHINA
[2] YUNNAN KEY LABORATORY OF SINO-GERMAN BLUE MINING AND UTILIZATION OF SPECIAL UNDERGROUND SPACE, KUNMING 650093, CHINA
[3] UNIVERSITY OF SCIENCE AND TECHNOLOGY BEIJING, BEIJING 100083; CHINA
[4] YUNNAN TECHNOLOGY AND BUSINESS UNIVERSITY, YANGLIN, YUNNAN 651701, CHINA

* Corresponding author: kmustsw@qq.com

1. Introduction

The rapid development and utilisation of mineral resources have provided a basic guarantee for the rapid development of China's economy. At the same time, due to the restriction of development level and economic conditions, China has paid a considerable price in terms of environment and safety [1-2]. At present, the tailing stock formed by mining and dressing in China reaches 14.6 billion tons, covering an area of 8700 km^2, equivalent to the area four times the size of Shenzhen. The construction of a tailings pond to accumulate tailings not only occupies a large amount of land resources but also needs to invest significant costs to ensure the safety of the tailings pond [3]. With the proposal and practice of the concept of "green water and green mountains," the construction of green mines has become the trend of future mine development [4]. With the continuous mining of metal ore resources, shallow mineral resources are gradually exhausted, and metal ore mining is transferred to deep mining. The following ground pressure management is the key technical problem faced by deep mining. The filling mining method can not only improve the stress state of surrounding rock and maintain the stability of the mined-out area, but also effectively solve the surface ecological environment problems caused by mining [5], which is the key to solving the problems of deep mining. According to the incomplete statistics of literature, China has more than 300 iron ore mines mined by the fill-and-fill mining method [6]. As the most crucial mining method in the world, the key technology of filling mining is the preparation and transportation of filling slurry and the strength of backfill [7]. Influenced by many factors, horizontal and inclined stratification surfaces will appear in the backfill, weakening the overall strength of the backfill, as shown in Fig. 1.

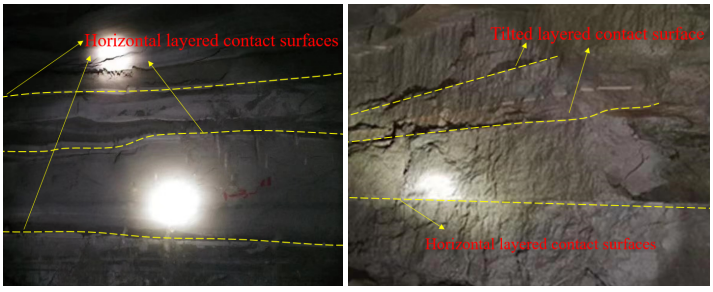

Fig. 1. Layered surface of the backfill

Many scholars have also done many studies on the layering and tilt of the filler. Li et al. [8] study the mechanical and microstructural characteristics of cementitious backfill (CB) with fly ash-FA, desulfurisation gypsum-DG, and steel slag-SS studied by both uniaxial compressive strength (UCS) and scanning electron microscope test; Gao et al. [9] analysis of Micro-crack Evolution and Failure Mode of Cut-tailed Sand-layered Backfill by PFC 3D Simulation; Wang et al. [10] study the effects of interface roughness and interface angle on the mechanical properties and damage evolution of LCGB were using uniaxial compression test, acoustic emission (AE) and digital image correlation (DIC). A numerical model of LCGB was built using simulation software (PFC2D) to demonstrate the dynamic crack evolution of LCGB during loading.; Jiao et al. [11] and Wang et al. [12] proved the reduction effect of the number and Angle of the structural weak

surface formed by layering and filling on strength revealed; Wang et al. [13] established the damage evolution and constitutive model of backfill body by using damage mechanics theory considering delamination effect, and established the strength criterion of backfill body considering delamination effect; Liu et al. [14] use a new damage constitutive model based on energy dissipation was developed to describe the behaviour of rocks under cyclic loading, a study of the damage variable based on energy dissipation was introduced, and the damage evolution equations of two typical rock types were calculated from the results of uniaxial cyclic loading tests; Tan et al. [15] study the uniaxial compression tests of mortar specimens with different sand ratios and loading rates were carried out. The energy stored and dissipated was calculated, and the damage constitutive model based on energy was established and verified. In this paper, the relationship between the strength of layered backfill and the mass concentration and inclination angle between layers is studied experimentally. The energy variation law of crack initiation and propagation process of layered backfill samples is analysed by combining the J integral, and the macroscopic performance of cracks is analysed from the microscopic point of view.

2. Experimental materials and scheme

2.1. Experimental materials and equipment

The size fraction composition curve of unclassified tailings is shown in Fig. 2. Fig. 2 shows that the content of –200 mesh (–74 μ m) particles in the unclassified tailings is 78.527%. The cement used in the experiment is ordinary portland cement with a grade of P.O42.5 of Shilin brand, and the density of unclassified tailings is 3.08 t/m^3. The chemical composition content of the tailings is shown in TABLE 1.

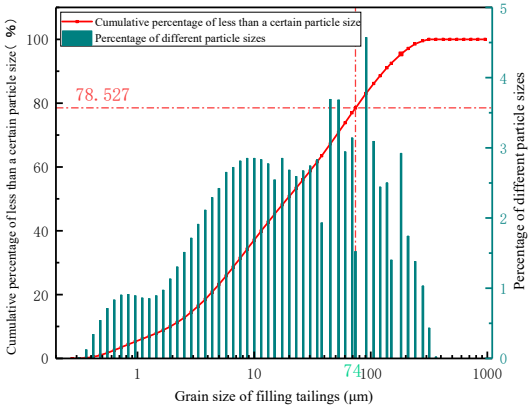

Fig. 2. Composition curve of whole tail sand grain level

It can be seen from TABLE 1 that the main chemical components of the unclassified tailings contain relatively high contents of SiO_2 and Fe_2O_3, and these oxides are generally not conducive to improving the strength of cemented backfill [16].

TABLE 1

Chemical composition of tail sand

Component content	Cu	Pb	Zn	Co	S	SiO_2	Al_2O_3	K_2O	Na_2O	CaO	Fe_2O_3	MgO	TiO_2	Others
(%)	0.058	0.14	0.048	0.005	5.07	37.87	5.85	1.88	0.20	6.56	28.58	2.38	1.34	10.019

A 300 kN micro-servo press was used as the experimental equipment, and the loading direction was from bottom to top (i.e. loading from the bottom layer), and the displacement-load data could be recorded in real-time. The experimental mould is a cylindrical mould with a standard electric flux of 50 mm × 100 mm.

2.2. Experiments and methods

During the actual filling of mine, due to the limitation of the filling process and filling parameters, different proportions are usually used for multiple filling, and the concentration of filling slurry changes accordingly [17]. In order to more significantly observe the influence of inclination angle and mass concentration on layered cemented backfill, the cement-sand ratio is set to 1:4. A group of 40 specimens with different interlaminar mass concentrations and inclined angles of 0°, 10°, 20° and 30° were tested under uniaxial compression. The height of each layer is 50 mm for the two-layer specimen; The height of each layer is 33.3 mm, and the sequence of

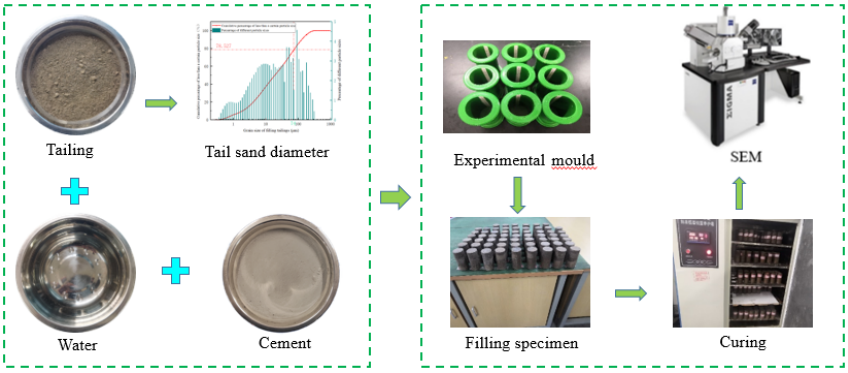

(a) Experimental flow chart

(b) stratified stratified samples

Fig. 3. Experimental flow and specimen diagram

mass concentration is 68%/67%/66%, representing the mass concentration of the top layer/middle layer/bottom layer. The filling interval is 24 h, and the constant temperature and humidity curing box is used for curing. The curing temperature is 20±1℃, the humidity is 95±5%, and the curing period is 28 days. The experimental procedures and test pieces are shown in Fig. 3.

The uniaxial compression results are shown in TABLE 2, by the data in TABLE 2 and Fig. 4 shows: that with the increase of contact Angle, the uniaxial compressive strength of the filling body specimen decreases; At a constant Angle, the strength of the filling body basic depends on the minimum mass concentration, three layered specimen strength is low, the strength of the minimum mass concentration at the bottom of the filling body is lower than in the strength of the filling body top.

3. Results and analysis

Analysing the data extraction in TABLE 2, the result is shown in Fig. 4.

TABLE 2

Uniaxial compressive strength of specimens with different inclination angles and interlaminar mass concentrations

Mass concentration /%	Uniaxial compressive strength (MPa)			
	0°	10°	20°	30°
68/67/66	3.39	3.27	3.09	2.79
68/66	3.43	3.35	3.21	3.07
68/66/68	3.62	3.54	3.41	3.15
66/67/68	3.72	3.59	3.46	3.18
67/66	4.00	3.85	3.69	3.41
66/67	4.19	4.07	3.88	3.58
68/67	4.35	4.20	4.03	3.78
68/67/68	4.71	4.55	4.45	4.19
66/68	5.07	4.85	4.61	4.33
67/68	5.25	5.13	4.89	4.53

3.1. Strength reduction coefficient of layered backfill

TABLE 2 illustrates that the uniaxial compressive strength of backfill is significantly weakened by the inclination angle [18]. The strength reduction factor is introduced here and defined as the formula (1):

$$K = \frac{\sigma_c'}{\sigma_c} \tag{1}$$

In formula (1), K is the strength weakening coefficient of layered cemented backfill; c is the compressive strength of backfill (MPa); c is the compressive strength (MPa) of the backfill with the inclination angle of 0°. The reduction factor of layered cemented fill is calculated based on the uniaxial compressive strength of the specimen with an inclination angle of 0° in TABLE 2, and the results are shown in TABLE 3.

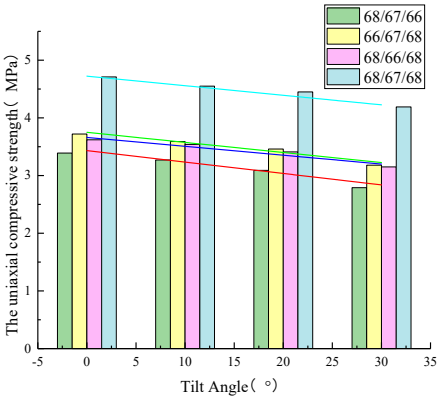

(a) concentration of three layered filling position

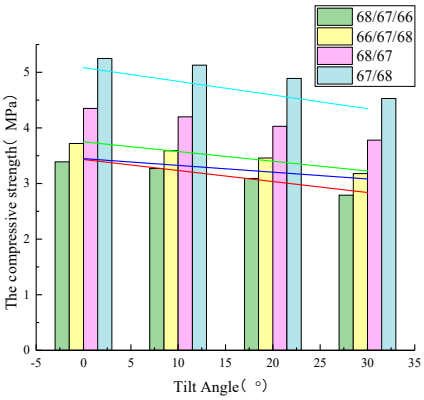

(b) different layers

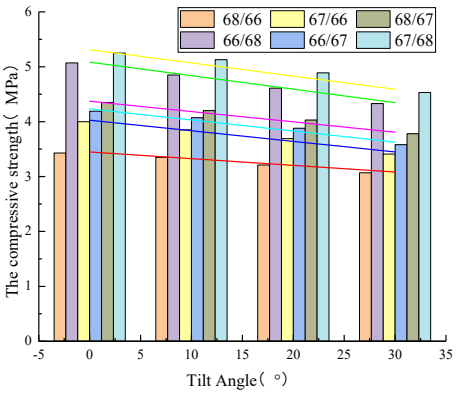

(c) concentration of two layered filling position

Fig. 4. Relationship between backfill strength under different factors

TABLE 3

Weakening coefficient of layered cemented filling strength

Mass concentration /%	**1:4**			
	0°	**10°**	**20°**	**30°**
68/67/66	1	0.96	0.91	0.82
68/66	1	0.98	0.94	0.90
68/66/68	1	0.98	0.94	0.87
66/67/68	1	0.97	0.93	0.85
67/66	1	0.96	0.92	0.85
66/67	1	0.97	0.93	0.85
68/67	1	0.97	0.93	0.87
68/67/68	1	0.97	0.94	0.89
66/68	1	0.96	0.91	0.85
67/68	1	0.98	0.93	0.86
mean value	1	0.97	0.93	0.86

It can be seen from TABLE 3 that the cosine values corresponding to the inclination angles of 10°, 20° and 30° of the backfill are cos10° = 0.98, cos20° = 0.94 and cos30° = 0.86, respectively, and the reduction coefficients of the uniaxial compressive strength of the corresponding angles in TABLE 3 are 0.97, 0.93 and 0.86, respectively, with good fitting effect, i.e., the uniaxial compressive strength of the backfill is positively correlated with the cosine value of the inclination angle of the backfill [19]. It can be seen from Fig. 5 that when the mass concentration between filling layers is constant, the strength reduction coefficient k decreases with the increase of the contact surface inclination angle, the greater the inclination angle, the clearer the weakening effect of compressive strength of backfill [20].

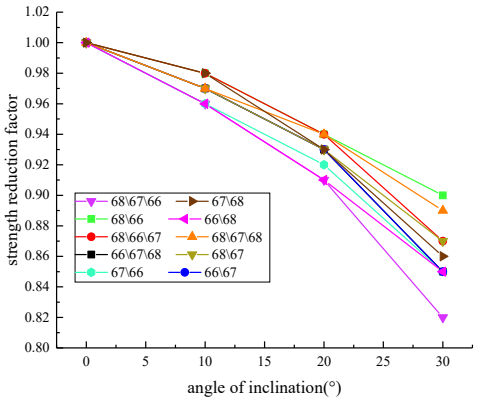

Fig. 5. Weak coefficient change curve with tilt angle

3.2. Analysis of influence of inclination angle on strength

Fig. 6 is cemented tailings backfill under a different mass concentration layer between the uniaxial compressive strength and the mass concentration and the relationship between the dip Angle.

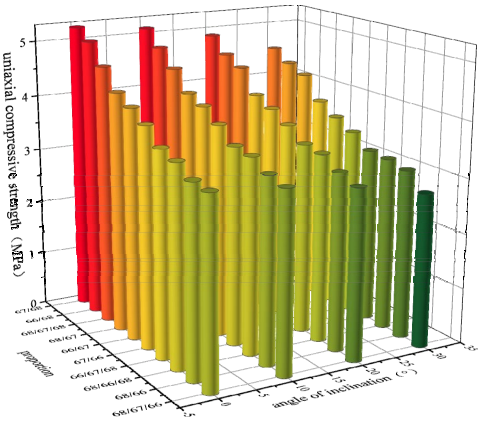

Fig. 6. The relationship between different conditions and the strength of the backfill

It can be seen from Fig. 6 that the inclination angle, the number of fillings and the mass concentration of the interlayer all affect the strength of the backfill. The strength of the bottom layer of the filler with minimum mass concentration is lower than that of the top layer of the filler, such as: $\sigma_{67/66} < \sigma_{66/67}$, $\sigma_{68/67} < \sigma_{67/68}$, $\sigma_{68/67/66} < \sigma_{66/67/68}$; With the increase of the number of layers, the strength of backfill decreases [21].

4. Analysis of specimen failure and energy characteristics

The failure condition (crack, contact surface dislocation, etc.) of the specimen can often directly reflect the strength of filling materials with different mass concentrations in the process of uniaxial compression, and the specimen with low strength is more likely to generate cracks to release energy [22]. Therefore, the phenomenon of low strength of low concentration material in the bottom of the backfill can be well explained by the study of the energy release rate of crack and energy transfer process of layered backfill.

4.1. Specimen energy characteristic

The deformation of the backfill unit under the action of uniaxial compression external force, assuming that there is no heat exchange with the outside world in this physical process, according to the law of conservation of energy, there is the following relationship [23]:

$$U = U^d + U^e \tag{2}$$

$$U = \int_0^{\varepsilon_1} \sigma_1 d\varepsilon_1 + \int_0^{\varepsilon 2} \sigma_2 d\varepsilon_2 + \int_0^{\varepsilon 3} \sigma_3 d\varepsilon_3 \tag{3}$$

$$U_e = \frac{1}{2}\sigma_1 \varepsilon^e = \frac{1}{2E_u}\sigma_1^2 U_e \tag{4}$$

In formulae (2)-(4): U is the total work done by the external force; U^d is the unit dissipation energy; ε is the deformation of the specimen under triaxial compression; U^e is the releasable elastic strain energy of the element, as shown in Fig. 7.

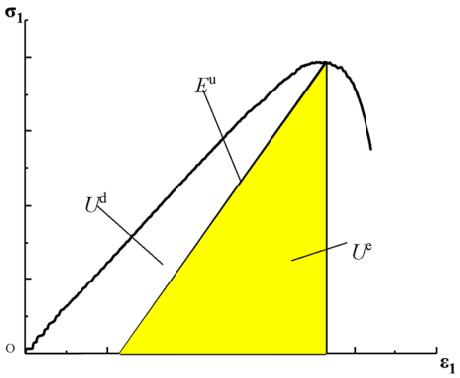

Fig. 7. Disdissipative and elastic strain energy in stress-strain curve [24]

In uniaxial compression $\sigma_2 = \sigma_3 = 0$, Equation (3) can then be expressed as:

$$U = \int_0^{\varepsilon_1} \sigma_1 d\varepsilon_1 \tag{5}$$

Substituting E_0 for E^u, then equation (4) can be expressed as:

$$U^e \approx \frac{1}{2E_0}\sigma_1^2 \tag{6}$$

In the formulae (5)-(6), E^u is the unloading elastic modulus, ε and σ are the stress and strain of the backfill specimen, respectively.

By substituting equations (5) and (6) into equation (2), the magnitude of the unit dissipation energy U^d at the time of loading can be calculated. The element dissipation energy is the reason for the formation of internal damage (such as cracks) and plastic deformation [25].

4.2. Analysis of J-integral variation based on homogeneous medium

In a homogeneous medium, any crack begins at any point on the lower surface, moves counterclockwise (positive of arc length s) around the crack tip, and terminates on the upper surface (when analysing the failure of an un-delaminated specimen). The J-integral of Rice is defined as [26]:

$$J = \int_\Gamma (Wdy - T \cdot \frac{\partial u}{\partial x} ds) \tag{7}$$

In formula (7), W is the strain energy density of the backfill; T is the external force vector acting on the Γ arc element ds of the integral loop; U is the displacement vector on the Γ loop where the x-axis is along the crack direction and the y-axis is perpendicular to the crack direction. When the uniform backfill specimen is subjected to a fixed external force, the energy release rate is [27]:

$$J = 8aW_0 \tag{8}$$

In Equation (8), a is the crack length and W_0 is the strain energy density without a crack. From the perspective of the total quantity theory, the J-integral is the rate of energy release of crack growth, i.e., the rate of change of the total potential energy with the change of the crack surface area, which is independent of the crack path.

4.3. Based on the analysis of *J*-integral change in layered media

Taking two layered specimens as an example for analysis, if the split tip advances in the x direction in a uniform material coordinate system, the strain energy of the material will decrease accordingly [28].

When the materials A and B are different homogeneous materials A and B on both sides of the filler interface, then the interface can be seen as a defect, and the interface J-integral can

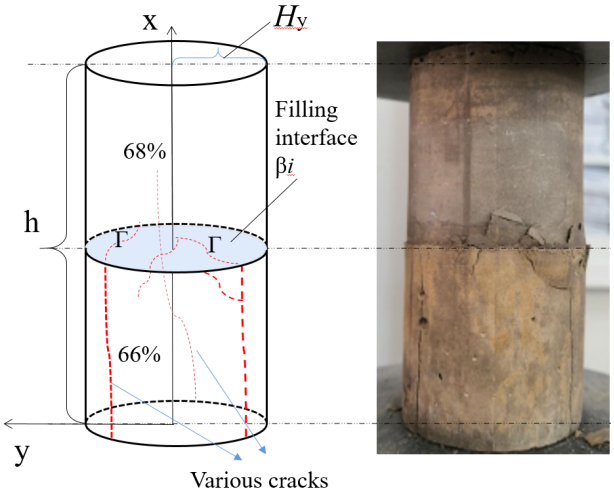

Fig. 8. *J*-integral path schematic

be seen as the force that drives the interface to move in the *x* direction, as shown in Fig. 8. The energy densities on both sides of the interface are respectively [29]:

$$W_{\mathrm{A}} = \frac{\sigma_{y\mathrm{A}}^2(1-V_{\mathrm{A}}^2)}{2E_{\mathrm{A}}} \tag{9}$$

$$W_{\mathrm{B}} = \frac{\sigma_{y\mathrm{B}}^2(1-V_{\mathrm{B}}^2)}{2E_{\mathrm{B}}} \tag{10}$$

In the formulas (9)-(10), E is the elastic modulus of the material; V is the Poisson's ratio of the material; y is the residual stress of each layer. If the diameter (i.e. thickness) of each layer of the backfill test piece is equal and the elastic modulus of layer A and layer B is the same, then the absolute value of residual stress of layer A and layer B is equal, and the strain energy density W on both sides of each interface is equal, resulting in the J integral of each interface being equal to 0 [30]. In this case, the layered backfill can be regarded as a uniform material, and the energy release rate of the crack can be directly calculated from Equation (8), which is independent of the crack path.

In the actual filling, the layered backfill will have different thicknesses. When the elastic modulus of layer A and layer B is different and the thickness is different, the difference of J integral between when the crack passes through the AB interface and when it does not pass through the interface is [31]:

$$J_{\Delta\beta i} = 2\int_0^{H_{yi}} \left[\left(W_0(x_{ia},y) - W_0(x_{ib},y)\right) - \left(W_a(x_{ia},y) - W_a(x_{ib},y)\right)\right] dy \tag{11}$$

In the formula (11), W_a represents the strain energy density when a crack is present, H_{yi} represents a physical quantity related to the thickness of the test piece, and i represents the i^{th} interface. x_{ia} and x_{ib} represent the lower side and upper side of the ith interface respectively, $x_{ia} = x_{ib} = x_i$,

x_i represents the x value of the i^{th} interface, and $J_{\Delta\beta i}$ is the release amount of energy transfer by the layered interface, which may cause interface separation dislocation, as shown in Fig. 10. $J_{f(0)}$ and $J_{f(a)}$ represent the J integrals along the same far-field path without and with a crack, respectively, and the same is true for J_c.

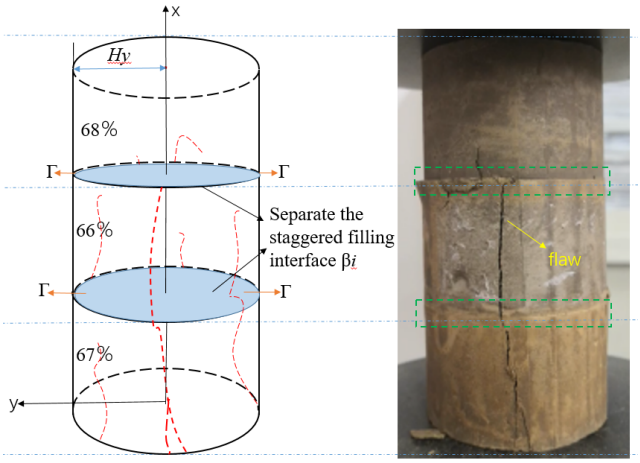

Fig. 9. Specimen destruction diagram

The relationship between the J integral of the crack tip and the far field J integral J_f and the interface J integral J_c is [32-35]:

$$J_t = J_{f(a)} - J_{c(a)} \tag{12}$$

in that absence of crack,

$$J_{f(0)} = J_{c(0)} \tag{13}$$

$$J_{c,i(0)} = 2H_{yi}\left\{\left|\frac{\sigma^2_{yB(1-V_B^2)}}{E_B} - \frac{\sigma^2_{yA(1-V_A^2)}}{E_A}\right|\right\} \ (i = 1,2,3...) \tag{14}$$

$$J_{c,i(0)} = J_{c,i(a)} - J_{\Delta\beta i} \tag{15}$$

$$J_{f(a)} - J_{f(0)} = 2\int_{L_i}(W_a - W_0)dy \tag{16}$$

In formula (14), H_{yi} represents half of the thickness of the material at the i^{th} interface, and:

$$J_t = \left(J_{f(a)} - J_{c(0)}\right) - J_{\Delta\beta i} \tag{17}$$

$$J_{c,i(0)} = 2H_{yi}\left|(W_B - W_A)\right| \tag{18}$$

In formula (16)-(17), L_i represents the circumference of the i^{th} layered circle with the crack length as the radius, J_t is the crack energy release rate, $J_{f(a)} - J_{c(0)}$ equal to the integral of the strain energy density release along the boundary $x = 0$. Therefore, the energy release rate of an edge crack in a layered material is equal to the integral of the strain energy density release along the boundary minus the change in the *J*-integral of the interface [36].

From the above analysis, it can be seen:

(1) Substitution (2) from equations (5) and (6) can calculate the unit dissipation energy that forms internal damage and plastic deformation of the backfill during loading U^d.

(2) The *J* integral is the energy required to generate a crack per unit area, and the energy required to fill the body before and after the crack reaches the interface β_i and the energy consumed at the interface β_i can be calculated by formulas (9), (10), (11), (14), (16), (17). From this, it follows that the energy absorbed by the material away from the loading direction decreases layer by layer with the number of layers.

(3) It can be seen from equations (9), (10) and (14) that the *J* integral of the filler can be expressed by the uniaxial compressive strength that the specimen can bear, so when the filler is inclined, its strain energy density changes correspondingly, that is, the crack energy release rate is related to its strength after being weakened by inclination.

4.4. Microcrack growth analysis

The compression failure of the backfill specimen with an interlaminar mass concentration of 68%/66%/68% and the crack propagation process of the specimen under numerical simulation are shown in the four stages A, B, C, and D, as shown in Fig. 10.

As can be seen from Fig. 10, A phase of the displacement is zero, basic didn't produce shear cracks contact area; Phase B layer contact surface to produce a small amount of shear crack, mutual penetration, development of micro-cracks between particles gradually form the macroscopic crack; Phase C shear crack propagation speed slows down, pull stress concentration at the shear crack, and with the increase of load, appear a lot of pressure, a tensile crack between particles, and gradually formed through the macro tensile crack; Phase D stress drops rapidly, displacement and crack increased rapidly. The whole damage process of cracks from the middle layer and the bottom of the interface, gradually to the middle layer at the top of the extension and extension, and even damage. Tensile crack from the numerical simulation of two layers of contact surfaces of the specimens produced at the same time, and as the pressure loading gradually extends to the middle [37].

5. Conclusion

Through the uniaxial compression test of the specimens with different mass concentrations and different inclined angle filling interfaces, the weakening effect of the inclined angle on the filling interface is analysed. Based on the *J* integral, the energy release of the crack and the separation and dislocation of the filling interface are studied:

(1) In a certain range of dip angle, the uniaxial compressive strength of the backfill decreases with the increase of dip angle, and the weakening effect of the specimen is more pronounced with the increase of dip angle, and the weakening coefficient is in good agreement with the cosine value of the corresponding dip angle.

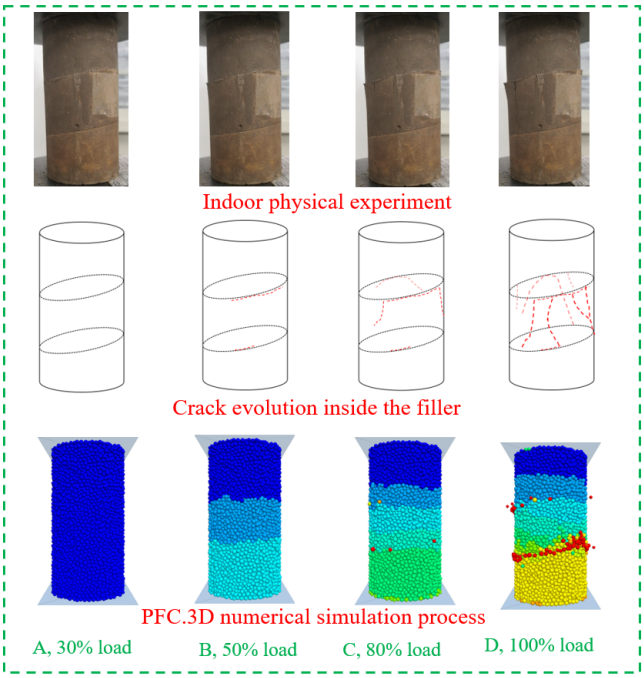

Fig. 10. Crack evolution process in indoor experiment and numerical simulation experiment

(2) When the dip angle is constant, the strength of the backfill decreases with the increase of layers. Its uniaxial compressive strength basically depends on the minimum interlayer mass concentration of the filler.

(3) The filling position of the minimum concentration has a significant influence on the strength of the backfill, and the energy transfer of the layered backfill has a decreasing trend during uniaxial compression. Generally, the farther the minimum mass concentration is from the loading direction, the greater the uniaxial compressive strength of the backfill, such as $\sigma_{66/68}/\sigma_{68/66} = 1.48$, $\sigma_{66/67/68}/\sigma_{68/67/66} = 1.10$.

(4) In the case of uniaxial compression, cracks generally begin to appear in the loading direction, and the interface separation dislocation occurs at the delamination interface. The crack usually starts from the interface of delamination and propagates. The energy consumed by crack propagation and interface dislocation makes the delamination far away from the loading direction not crack or only a few cracks. Therefore, in the actual filling, we can optimise the different interlayer mass concentrations to improve the stability of the backfill, and calculate the number of cracks and strain energy consumption in the backfill by monitoring the displacement of the backfill so as to maintain the safety of the stope.

Declaration of Competing Interest

The authors declare that they have no known competing financial interests or personal relationships that could have appeared to influence the work reported in this paper.

Acknowledgments

This research was financially supported by different research funds: National Natural Science Foundation of China (Grant No. 51964023), the Yunnan Major Scientific and Technological Projects (Grant No. 202202AG050014), the Yunnan Fundamental Research Projects (Grant No. 202101BE070001-038;202201AT070146).

References

[1] M. Sari, E. Yilmaz, T. Kasap, et al. Exploring the link between ultrasonic and strength behavior of cementitious mine backfill by considering pore structure. Constr. Build. Mater. **370**, 130588 (2023). DOI: https://doi.org/10.1016/j.conbuildmat.2023.130588

[2] W. Sun, H.J. Wang, K.P. Hou, Control of waste rock-tailings paste backfill for active mining subsidence areas. J. Clean. Prod. **171**, 567-579 (2018). DOI: https://doi.org/10.1016/j.jclepro.2017.09.253

[3] H.Y. Cheng, J. Liu, S.C. Wu, XQ Zhang, Fluidization Analysis of Thickening in the Deep Cone for Cemented Paste Backfill. Adv. Mater. **27**, 6285981 (2020). DOI: https://doi.org/10.1155/2020/6285981

[4] H. Cao, Q. Gao, X.Z. Zhang, et al., Research Progress and Development Direction of Filling Cementing Materials for Filling Mining in Iron Mines of China. Gels. **3**, 192 (2022). DOI: https://doi.org/10.3390/gels8030192

[5] D.L. Gong, X.G. Yang, S.C. Qi, et al., Coupled chemo-hydro-mechanical effects in one-dimensional accretion of cemented mine fills. Eng. Geol. **267**, 105495 (2020). DOI: https://doi.org/10.1016/j.enggeo.2020.105495

[6] X.B. Li, W. Wei, B. Zhao, Construction and Quantitative Analysis of Evaluation Index System on Stability of Filling System. J. Eng. Sci. Technol. Rev. **31** (31), 43-47 (2013). http://www.kjdb.org/CN/10.3981/j.issn.1000-7857.2013.31.006

[7] W. Sun, A.X. Wu, K.P. Hou, et al., Real-time observation of meso-fracture process in backfill body during mine subsidence using X-ray. CT under uniaxial compressive conditions. Constr. Build. Mater. **113**, 153-162 (2016). DOI: https://doi.org/10.1016/j.conbuildmat.2016.03.050

[8] J.J. Li, E. Yilmaz, S. Cao, Influence of industrial solid waste as filling material on mechanical and microstructural characteristics of cementitious backfills. Constr. Build. Mater. **299**, 124288 (2021). DOI: https://doi.org/10.1016/j.conbuildmat.2021.124288

[9] T. Gao, W. Sun, Z. Liu, et al., Investigation on fracture characteristics and failure pattern of inclined layered cemented tailings backfill. Constr. Build. Mater. **343**, 128110 (2022). DOI: https://doi.org/10.1016/j.conbuildmat.2022.128110

[10] Y.M. Wang, J.Y. Wu, H. Pu, et al., Effect of interface geometric parameters on the mechanical properties and damage evolution of layered cemented gangue backfill: Experiments and models. Constr. Build. Mater. **349**, 128678 (2022). DOI: https://doi.org/10.1016/j.conbuildmat.2022.128678

[11] H.Z. Jiao, W.B. Yang, H.M. Shen, et al., Study on Multi-Layer Filling Treatment of Extra-Large Goaf and Its Underground Application. Materials **16**, 5680 (2022). DOI: https://doi.org/10.3390/ma15165680

[12] J.J. Li, E. Yilmaz, S. Cao, Influence of solid content, cement/tailings ratio and curing time on rheology and strength of cemented tailings backfill. Minerals **10** (10), 922 (2020). DOI: https://doi.org/10.3390/min10100922

[13] J. Wang, W.D. Song, S. Cao, et al., Mechanical properties and failure modes of stratified backfill under triaxial cyclic loading and unloading. Int. J. Min. Sci. Technol. **29**, 809-814 (2019). DOI: https://doi.org/10.1016/j.ijmst.2018.04.001

[14] X.S. Liu, J.G. Ning, Y.L. Tan, et al., Damage constitutive model based on energy dissipation for intact rock subjected to cyclic loading. Int. J. Min. Sci. Technol. **85**, 27-32 (2016). DOI: https://doi.org/10.1016/j.ijrmms.2016.03.003

[15] Y.L. Tan, Q.H. Gu, J.G. Ning, et al., Uniaxial Compression Behavior of Cement Mortar and Its Damage-Constitutive Model Based on Energy Theory. Materials **12**, 1309 (2019). DOI: https://doi.org/10.3390/ma12081309

[16] W.D. Song, J. Wang, Y.Y. Tan, et al., Energy consumption and damage characteristics of layered filling under triaxial addition-unloading. Int. J Min. Sci. Technol. **46** (05), 1050-1057 (2017). DOI: https://doi.org/10.13247/j.cnki.jcumt.000738

[17] B. Han, S.Y. Zhang, W. Sun, Impact of Temperature on the Strength Development of the Tailing-Waste Rock Backfill of a Gold Mine. Adv. Civ. Eng. Mater. **10** (1155), 4379606 (2019). DOI: https://doi.org/10.1155/2019/4379606

[18] W. Sun, M.G. Jiang, K. Fan, Z. Liu, Determination and Application of Pressure Loss in Long Distance Pipeline Transportation of Paste Slurry Based on Pipe Loop Experiment. Arch. Min. Sci. **67**, 2, 223-237 (2022). DOI: https://doi.org/10.24425/ams.2022.141455

[19] K.F. Lu, W. Sun, T. Gao, et al., Preparation of new copper smelting slag-based mine backfill material and investigation of its mechanical properties [J]. Constr. Build. Mater. **382**, 131228 (2023). DOI: http://dx.doi.org/10.1016/j.conbuildmat.2023.131228

[20] Z.Y. Li, W. Sun, T. Gao, et al., Experimental study on evolution of pore structure of inclined layered cemented tailings backfill based on X-ray CT. Constr. Build. Mater. **366**, 130242 (2023). DOI: https://doi.org/10.1016/j.conbuildmat.2022.130242

[21] T. Gao, W. Sun, Z.Y. Li, et al., Study on Shear Characteristics and Failure Mechanism of Inclined Layered Backfill in Mining Solid Waste Utilization. Minerals **12** (12), 1540 (2022). DOI: https://doi.org/10.3390/min12121540

[22] H.Z. Jiao, W. Zhang, Y. Yang, et al., Static mechanical characteristics and meso-damage evolution characteristics of layered backfill under the condition of inclined interface. Constr. Build. Mater. **366**, 130113 (2023). DOI: https://doi.org/10.1016/j.conbuildmat.2022.130113

[23] H.Z. Jiao, W.X. Zhang, Y.X. Yang, et al., Static mechanical characteristics and meso-damage evolution characteristics of layered backfill under the condition of inclined interface. Constr. Build. Mater. **366**, 130113 (2023). DOI: https://doi.org/10.1016/j.conbuildmat.2022.130113

[24] J. Deng, B. Li, X.B. Li. et al., Analysis of factors and countermeasures of mining subsidence in Kaiyang Phosphorus Mine. J. Cent. South Univ. Technol. **13**, 733-737 (2006). DOI: https://doi.org/10.1007/s11771-006-0023-7

[25] X.P. Song, J.B. Li, S. Wang, et al., Study of mechanical behavior and cracking mechanism of prefabricated fracture cemented paste backfill under different loading rates from the perspective of energy evolution. Constr. Build. Mater. **361**, 129737 (2022). DOI: https://doi.org/10.1016/j.conbuildmat.2022.129737

[26] J. Wang, J.X. Fu, W.D. Song, et al., Mechanical properties, damage evolution, and constitutive model of rock-encased backfill under uniaxial compression. Constr. Build. Mater. **285**, 122898 (2021). DOI: https://doi.org/10.1016/j.conbuildmat.2021.122898

[27] W.Y. Qi, J.X. Zhang, N. Zhou, et al., Mechanism by Which Backfill Body Reduces Amount of Energy Released in Deep Coal Mining. Shock and Vibration **14**, 8253269 (2019). DOI: https://doi.org/10.1155/2019/8253269

[28] L. Liu, J. Xin, C.C. Qi, et al., KI-IL Song, Experimental investigation of mechanical, hydration, microstructure and electrical properties of cemented paste backfill. Constr. Build. Mater. **263**, 120137 (2020). DOI: https://doi.org/10.1016/j.conbuildmat.2020.120137

[29] S. Xiao, H.L. Wang, B. Liu, et al., The surface-forming energy release rate based fracture criterion for elastic-plastic crack propagation. J. Mech. Phys. Solids. **84**, 336-357 (2015). DOI: https://doi.org/10.1016/j.jmps.2015.08.011

[30] T. Nishioka, S.S. Syano, T. Fujimoto, Concepts of Separated J-Integrals, Separated Energy Release Rates, and the Component Separation Method of the J-Integral for Interfacial Fracture Mechanics. J. Appl. Mech. **70** (4), 505-516 (2003). DOI: https://doi.org/10.1115/1.1576803

[31] T. Nishioka, S.P. Shen, J.H. Yu, Dynamic *J* integral, separated dynamic *J* integral and component separation method for dynamic interfacial cracks in piezoelectric bimaterials. Int. J. Fract. **122**, 101-130 (2003). DOI: https://doi.org/10.1023/b:frac.0000005768.61301.a7

[32] L.K. Lu, Z.L. Liu, Z. Zhuang, The physical meanings of two incremental-J-integral-based fracture criteria for crack growth in elastic-plastic materials. Eng. Fract. Mech. **259**, 108106 (2022). DOI: https://doi.org/10.1016/j.engfracmech.2021.108106

[33] C.R. Chen, Analysis on the Energy Release Rate Considering the Difference Between J-Integrals With and Without a Crack [J]. Applied J. Math. Mech. **39** (10), 1172-1179 (2018). DOI: https://doi.org/10.21656/1000-0887.380191

[34] Z. Chen, R.D. Adams, Lucas F.M. da Silva, Prediction of crack initiation and propagation of adhesive lap joints using an energy failure criterion. Eng. Fract. Mech. **78** (6), 990-1007 (2011). DOI: https://doi.org/10.1016/j.engfracmech.2010.12.004

[35] A. Pirondi, C.D. Donne, Characterisation of ductile mixed-mode fracture with the crack-tip displacement vector. Eng. Fract. Mech. **68** (12), 1385-1402 (2001). DOI: https://doi.org/10.1016/S0013-7944(01)00023-6

[36] W. Liu, S.L. Xu, Q.H. Li, Experimental study on fracture performance of ultra-high toughness cementitious composites with J-integral. Eng. Fract. Mech. **96**, 656-666 (2012). DOI: https://doi.org/10.1016/j.engfracmech.2012.09.007

[37] W. Sun, T. Gao, J.G. Zhao, et al., Research on fracture behavior and reinforcement mechanism of fiber-reinforced locally layered backfill: Experiments and models. Constr. Build. Mater. **366**, 130186 (2023). DOI: https://doi.org/10.1016/j.conbuildmat.2022.130186